Journal of Computers Vol. 34 No. 6, December 2023, pp. 153-162
doi: 10.53106/199115992023123406012

Research on Three Common Fault Diagnosis Methods for AC Asynchronous Motors Based on Deep Learning

Mu-Zhuo Zhang, Peng-Jie Du*

School of Automation Engineering, Tangshan Polytechnic College,
Tangshan City 063299, Hebei Province, China
{zmz19920923, dpj20220701}@126.com

Received 1 October 2023; Revised 1 November 2023; Accepted 13 December 2023

Abstract. In response to the problem that traditional fault diagnosis methods mainly rely on manual search, this paper proposes an improved convolutional neural network based three item asynchronous motor fault diagnosis method. Taking the motor rotor bar fault as the research object, in the early stage of the fault, the characteristic signal is easily mixed with the motor fundamental frequency signal. Therefore, first, the current characteristics of the motor rotor bar fault are analyzed, and then the motor vibration signal is converted into a time-frequency map using wavelet analysis method. Then, based on the superpixel segmentation method, the image is generated into a superpixel block. Finally, the image information is input into an improved neural network, The improved neural network can adaptively extract fault features. The experimental results show that the method described in this article can improve the diagnostic ability for rotor bar breaking faults, and has a higher fault recognition accuracy compared to traditional methods.

Keywords: CNN, intelligent diagnosis, motor fault, broken rotor bar

1 Introduction

Three phase asynchronous motors have been widely used in contemporary industrial production processes due to their advantages of stable performance and low price. Long term operation of motors in complex industrial environments is prone to various faults, ranging from economic losses to threats to personal safety. If we can predict motor faults in a timely manner before they occur, and diagnose and repair faults quickly and accurately when they occur, we can reduce the losses caused by such sudden accidents. Therefore, conducting in-depth and detailed research on fault diagnosis methods for three-phase asynchronous motors and exploring more accurate and efficient fault diagnosis methods is of great significance.

With the development of artificial intelligence, intelligent fault diagnosis technology has shown significant advantages over traditional fault detection methods. However, the current algorithm still has shortcomings, such as requiring a large number of training samples, being prone to falling into local minima, long learning time, and slow convergence speed. The work done in this article is to combine fault diagnosis of three-phase motors with intelligent algorithms as follows:

1) By conducting in-depth research on the fault mechanism of three-phase asynchronous motors through finite element analysis and other means, establish an accurate motor fault diagnosis model;

2) To address the shortcomings of premature convergence and tendency to fall into local optima in particle swarm optimization, the algorithm is improved, and then the improved particle swarm algorithm is used to diagnose motor faults;

3) Establish a real experimental environment and validate the method proposed in this paper.

In summary, the composition and structure of the article are as follows: Chapter 2 mainly introduces the relevant work of scholars in fault diagnosis, improvement algorithms, etc. Chapter 3 introduces the fault analysis and modeling process of motor rotor bars. Chapter 4 is an improvement on existing intelligent diagnosis algorithms. Chapter 5 sets up an experimental environment and verifies the feasibility of the proposed method. Chapter 6 is the conclusion section.

* Corresponding Author

2 Related Work

Marmouch Same proposes a technology that combines motor current analysis with artificial intelligence for motor fault identification, and implements fault detection based on neural networks and probabilistic neural networks for motor current analysis [1]. Jeongho Kang identifies the sound characteristics of different noises by listening for the noise emitted by the engine and using improved noise integral recognition technology, thereby accurately determining the type and location of faults [2]. Jiabin Wen mainly studied the fault characteristics of brushless DC motors, selecting the three wire current signal and the bus current signal of the brushless DC motor as diagnostic signals, and then using a deep residual network for feature recognition, the recognition accuracy can reach over 94% [3]. Liang Han proposed a fault diagnosis method for asynchronous motors based on an improved BP algorithm, which can not only classify and recognize the four fault states of the motor, but also improve the convergence speed of the network and reduce the probability of the algorithm falling into local minima [4]. Wenwei Cai, in order to diagnose the initial faults of micro motors, based on the characteristics of fault noise, uses convolution wavelet threshold denoising method to enhance the periodic impact components in the sound signal and filter out environmental noise. This method has good applicability [5]. Xuezhen Cheng proposed an adaptive neural fuzzy Petri net fault diagnosis method. Firstly, using Gaussian function instead of transition credibility, a system model is established and fault diagnosis is conducted based on the fault operation mechanism and fault characteristics of three-phase asynchronous motors. The simulation results show the efficiency of the algorithm [6].

3 Modeling of Rotor Bar Breaking Faults in Three Asynchronous Motors

In motor fault diagnosis, the analysis of fault mechanism and fault characteristics is the primary prerequisite for fault diagnosis. Based on the motor model to identify faults, by studying the electromagnetic principle of the motor, establish a fault model of the motor, analyze the changes in various physical quantities when the motor malfunctions, and thus achieve motor fault diagnosis.

3.1 Modeling and Analysis of Rotor Broken Bar Fault Based on Finite Element Method

The finite element method divides the computational domain into a finite number of non overlapping and interconnected small regions, which are called elements. Each small region has an element basis function, and the linear combination of the basis functions is used to approximate the true solution in the element [7]. The overall basis function can be seen as a combination of element basis functions, so the solution of the entire computational domain is composed of the approximate solutions of all elements. In the finite element calculation of electric motor electromagnetic fields, the calculation accuracy of two-dimensional electromagnetic fields can meet the requirements of engineering after experimental correction, and compared to three-dimensional fields, the calculation amount is small. Therefore, this article chooses to use two-dimensional electromagnetic fields for simulation analysis. The motor parameters are shown in Table 1.

Table 1. Motor parameter table

Motor parameters	Parameter value	unit
Outer diameter of stator	250	mm
Stator Bore	185	mm
Rotor outer diameter	180	mm
Inner diameter of rotor	79	mm
Number of stator/rotor slots	36/28	--
Core length	198	mm
Rated power	6.8	kW
Rated voltage	380	V
SPEED	960	r/min
Synchronous	1000	r/min
Number of pole pairs	3	--

Set the material and electromagnetic properties of each part of the motor, then perform finite element analysis and set the boundary conditions of the model, and finally perform computer solution and post-processing. Firstly, set the parameters of the stator, rotor, and each axis according to the motor parameter table, and establish the entity in the simulation software. The simulation model is shown in Fig. 1(a). Set the material of the motor stator core as silicon steel sheet; The material in the stator winding area is copper; The air gap area is air. Set the material property of the normal guide bar to copper bar and simulate partial broken bar faults by increasing magnetic permeability. When simulating complete broken bar faults, set the material property of the faulty guide bar to vacuum. The finite element model is shown in Fig. 2.

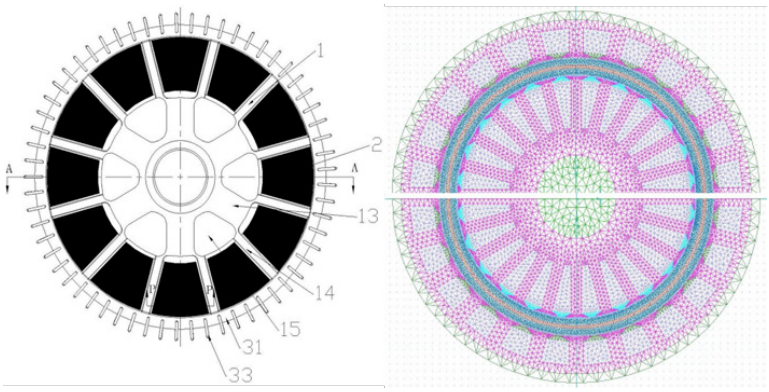

(a) 2D diagram of rotor (b) Finite element diagram of rotor

Fig. 1. Motor rotor

Select different cutting sizes to cut the stator, rotor, and iron core. When the rotor bar breaks, the air gap magnetic field of the motor is asymmetric, so it is necessary to solve the entire domain by setting the boundary condition $A_z = 0$ of the outer diameter of the stator. The motor is connected in a star configuration, and the three excitations are as follows:

$$\begin{cases} U_a = 220\sqrt{2}\sin(\omega t) \\ U_b = 220\sqrt{2}\sin\left(\omega t - \dfrac{2\pi}{3}\right) \\ U_c = 220\sqrt{2}\sin\left(\omega t + \dfrac{2\pi}{3}\right) \end{cases}. \tag{1}$$

The total solution often needs to be determined based on the requirements of later signal processing. According to the needs of subsequent fault signal extraction, the simulation time T is set to start from 0s and end at 3s. The simulation calculation time step is set to 0.0002s, which means the sampling frequency is 5000Hz.

3.2 Feature Extraction of Broken Bar Faults in Three Asynchronous Motors

When a motor experiences a broken rotor bar fault, a specific frequency component is induced in the stator current. When the steady-state running motor is affected by external interference and causes speed fluctuations, the characteristic frequency of the broken bar fault will also fluctuate, meaning that the fault characteristic signal is a signal distributed around a compact distribution. After singular value decomposition processing, the fundamental frequency and most of the noise in the original current signal have been removed. However, due to limitations in spectral resolution and speed fluctuations, the fault feature frequency can still be submerged, making it difficult to accurately extract the fault signal for diagnosis of broken bar faults. The successive variable mode decomposition (SVMD) method is used to reflect the frequency variation over time and has strong anti-interference abil-

ity. SVMD decomposes the original signal into a series of intrinsic mode functions by constructing and solving constrained variational problems, and adaptively matches the optimal center frequency of each mode. SVMD is equivalent to a set of bandwidth filters, which control the bandwidth of modes by setting penalty factors. Each mode is tightly distributed around its own central frequency, so SVMD can achieve effective separation of modes and frequency domain division of signals [8].

To verify the effectiveness of SVMD in extracting fault feature signals, the current waveform and spectrum distribution of a broken bar and a healthy motor processed by SVMD are used as examples, as shown in Fig. 2. The left side shows the current waveform and the right side shows the current spectrum. From Fig. 2(a) and Fig. 2(c), it can be seen that although the fundamental wave and most of the noise are filtered out after SVD processing, there is still interference from other frequencies. SVMD is used to decompose the processed current signal into a series of IMF sub signals distributed around their respective center frequencies. As shown in the spectra of Fig. 2(b) and Fig. 2(d), the frequency domain where the fault feature frequency is located is separated from other frequency domains through decomposition, further filtering out noise, and rotor bar breaking fault diagnosis is carried out based on the amplitude of the fault feature frequency.

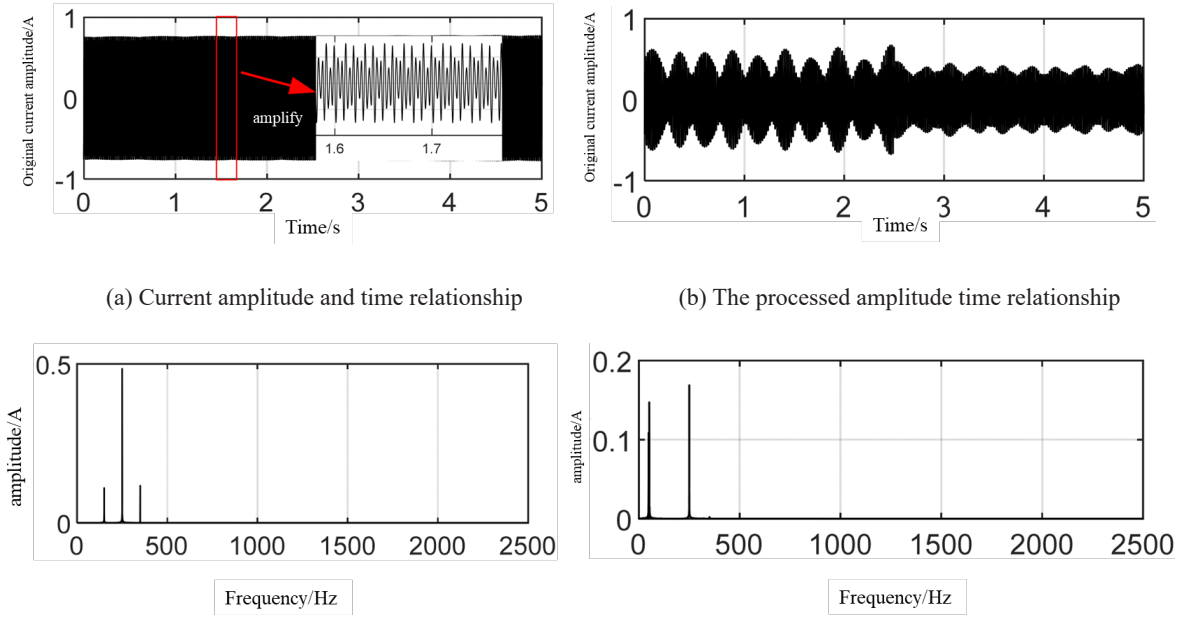

(a) Current amplitude and time relationship

(b) The processed amplitude time relationship

(c) Current amplitude and time relationship

(d) The processed amplitude time relationship

Fig. 2. Comparison of SVMD processing results

4 Establishment of Fault Diagnosis Model

4.1 Feature Extraction of Broken Bar Faults in Three Asynchronous Motors

This article uses wavelet packet analysis to perform more precise signal time-frequency analysis on motors. When the motor is in different fault states, wavelet packets are used to decompose the stator current signal of the motor, that is, one-dimensional signal processing [9]. The schematic diagram of wavelet packet decomposition is shown in Fig. 3.

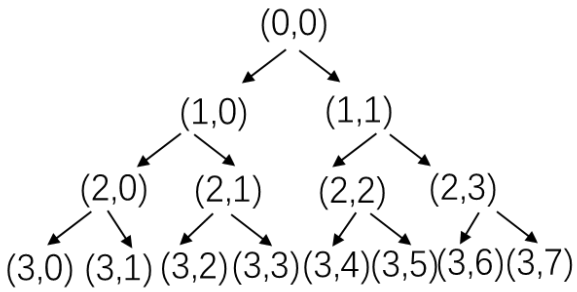

Fig. 3. Schematic diagram of small package decomposition

Each node represents a certain signal feature, while node (i, j) represents the j -th node of layer i , i = 0, 1, 2, 3, j = 0, 1, 2, 3, 4, 5, 6, 7. After decomposing and reconstructing the signal using the wavelet packet algorithm, the energy values in each frequency band can be calculated as the feature vectors of the signal. Assuming that the 3-th layer is processed using wavelet packet decomposition, the reconstructed signal in the j -th frequency band is represented by $S(3, j)$, and the corresponding signal energy is $E(3, j)$, it is represented as:

$$E(3, j) = \int \left| S(3, j)(t) \right|^2 dt = \sum_{k=1}^{n} \left| x_{kj} \right|^2. \tag{2}$$

In the formula, $x_{ij}(j = 0, 1, 2, ..., 7; k = 1, 2, ..., n)$ is the amplitude of the discrete points of the reconstructed signal $S(3, j)$, n is the number of signal sampling points, and E_3 is defined as the sum of the energy of each frequency band of signal $S(3, j)$, namely:

$$E_3 = \sum_{j=0}^{7} E(3, j). \tag{3}$$

In order to reduce the workload of algorithm iteration, the energy within each frequency band is normalized as follows:

$$E_{3j}^{*} = \frac{E(3, j)}{E_3}. \tag{4}$$

After energy normalization through formula 4, the extracted motor fault feature vector is represented as:

$$E_{3j}^{*} = \left(E_{30}, E_{31}, E_{32}, E_{33}, E_{34}, E_{36}, E_{37} \right). \tag{5}$$

4.2 Improved Neural Network Structure

A neural network has an input layer, a hidden layer, and an output layer. v_{ij} is the weight value from the input layer to the hidden layer, b_1 is the threshold value of the hidden layer, w_{jk} is the weight value from the hidden layer to the output layer, b_2 is the threshold value of the output layer, $h(\cdot)$ and $f(\cdot)$ are the transfer functions used by the hidden layer and output layer nodes, respectively. $X = [x_1, ..., x_i, ..., x_n]^T$ is the input of the network, and $O = [o_1, ..., o_k, ..., o_q]^T$ is the output of the network. The input and output relationship of the neural network can be expressed as:

$$o_k = f\left[\sum_{j=1}^{m} w_{jk} h(\sum_{i=1}^{n} v_{ij} x_i - b_1) - b_2\right] \quad i = 1,2,\cdots n; j = 1,2,\cdots,m; k = 1,2,\cdots,q. \tag{6}$$

The total error function of the network output is expressed as:

$$E = \frac{1}{p}\sum_{p=1}^{p}\sum_{k=1}^{q}(d_k^p - o_k^p)^2. \tag{7}$$

In the formula, p is the total number of samples included, and d is the expected output value of the network. Calculate the error signals of each layer based on the total error output of the network to adjust the weight of the network. Use an improved particle algorithm to search for the optimal weight [10].

4.3 Chaotic Dynamic Weighted Particle Swarm Optimization Algorithm

Due to the inherent problems of premature convergence and tendency to fall into local optima in particle swarm optimization, the improvements are as follows: inertia weight is a crucial parameter that determines the convergence speed, represented by w. The inertia weight gradually decreases with the increasing number of iterations, resulting in a decrease in the convergence speed and search accuracy of particle swarm optimization. Due to the ergodicity, non repeatability, and sensitivity of chaotic maps, they can perform search tasks faster than relying on probability to randomly search in space. Therefore, chaotic maps are applied to adjust dynamic weight w. The adjustment formula for w is:

$$w = x_k = u\left(7.86x_{k-1} - 23.31x_{k-1}^2 + 28.75x_{k-1}^3 - 13.302875x_{k-1}^4\right). \tag{8}$$

$$x_k \in (0,1); 0.9 < u < 1.08; k = 1,2,\cdots,M_{\max}. \tag{9}$$

In the formula, k is the number of iterations, and the local and global search abilities of particles are contradictory. In order to achieve better optimization performance of the algorithm, it is necessary to handle the local and global search abilities of particles well. Modify the position update method of particles to:

$$x_i^d = X_i^d \cdot w_{ij} + V_i^d \cdot w_{ij}^* + \rho \cdot g_{best}^d \cdot \Psi. \tag{10}$$

In the formula, w_{ij} and w_{ij}^* are dynamic weights used to adjust the image of the particle's previous position and velocity, g_{best}^d is the global optimal solution, which can accelerate the convergence speed of the algorithm after introduction, Ψ is the acceleration coefficient, which determines the maximum step size, ρ is the random number between [0,1], and w_{ij} , w_{ij}^* , and Ψ are defined as follows:

$$w_{ij} = \Psi = \frac{\exp[f(j)/u]}{\{1+\exp[-f(j)/u]\}^{iter}}. \tag{11}$$

$$w_{ij}^* = 1 - w_{ij}. \tag{12}$$

In the formula, A is the average fitness value of each particle during the first iteration, B is the current number of iterations, and C is the fitness value of the D-th particle. After the above analysis, the entire motor diagnosis flowchart is shown in Fig. 4.

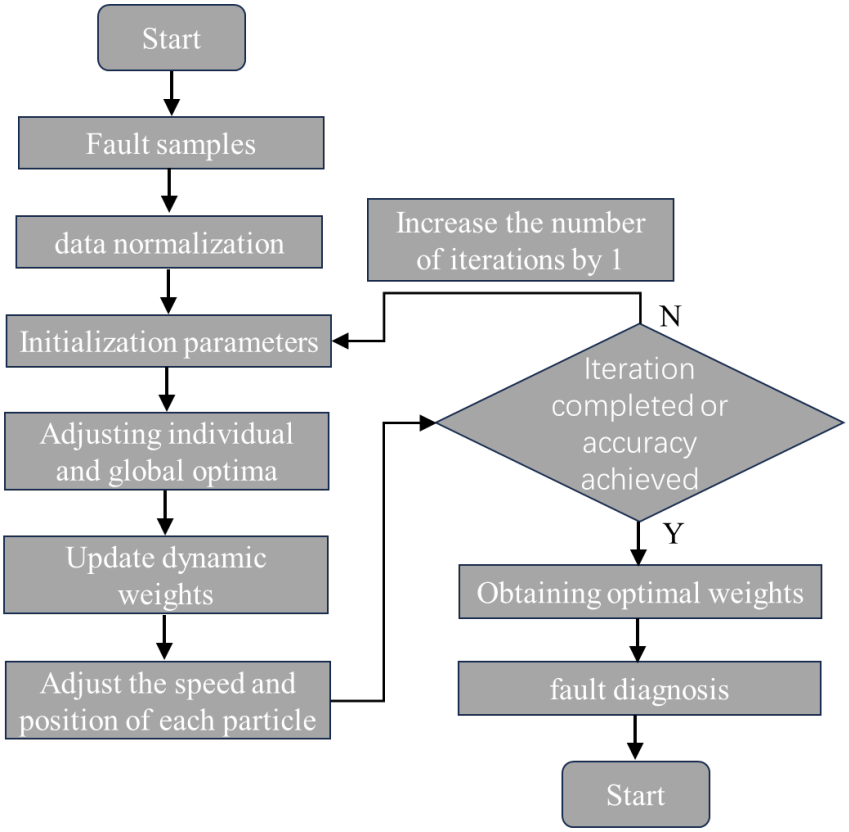

Fig. 4. Optimized intelligent diagnosis flowchart

5 Simulation Experiment and Result Analysis

Select two pole asynchronous motors 1.5kW, 50Hz, 380V, and 1450r/min for testing, and adjust the load changes using a dynamometer. The rotor broken bar fault is simulated by drilling holes in the rotor; The simulation of rotor eccentricity fault is achieved by directly installing a screw on the rotor mold and adding additional weight to disrupt the original vibration balance of the rotor, which will cause irregular vibration of the motor and achieve the effect of air gap eccentricity; Imbalance of three-phase voltage can cause the motor to be in an overload state for simulation. Set the rotor broken bars to 1 broken, 2 broken, and 3 broken, and set the data sampling frequency to 1kHz.

5.1 Fault Sample Selection

The sensor is used to detect the stator current signal of asynchronous motor $(1 \pm 2s)f$, and the raw data is obtained after preprocessing such as A/D data sampling. The original data of the motor in different states is decomposed and reconstructed using three-layer wavelet packets to obtain signal features in different frequency ranges of the third layer. Normalize the energy signals of each frequency band to form the fault feature vector E^* of the motor. The sampling frequency of the data is 1kHz, and the analysis upper limit frequency is set to 500Hz. The schematic diagram is shown in Fig. 5.

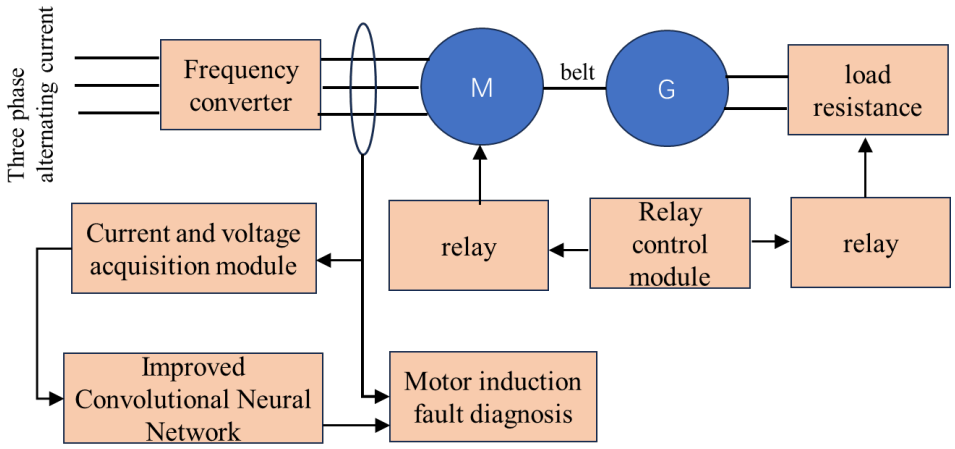

Fig. 5. Fault diagnosis schematic diagram

The training and testing sample dataset of the neural network is shown in Table 2.

Table 2. Fault diagnosis dataset

Sample	E_{30}	E_{31}	E_{32}	E_{33}	E_{34}	E_{35}	E_{36}	E_{37}	Q	Fault type
1	0.0328	0.0433	0.0712	0.0321	0.0312	0.0231	0.0898	0.4234	1	Motor is normal
2	0.0713	0.2192	0.1013	0.7212	0.3124	0.0872	0.1274	0.2348	2	1 broken bar
3	0.1256	0.1272	0.1312	0.1241	0.3216	0.3124	0.9871	0.8212	3	2 broken bar
4	0.1792	0.5012	0.1726	0.2124	0.2148	0.5134	0.2412	0.2314	4	3 broken bar
5	0.7009	0.1231	0.2121	0.1234	0.3821	0.3983	0.3872	0.6512	5	Rotor eccentricity
6	0.4012	0.0725	0.2981	0.4121	0.6129	0.7123	0.6896	0.1249	6	Voltage imbalance
⋮	⋮	⋮	⋮	⋮	⋮	⋮	⋮	⋮	⋮	⋮
700	0.1701	0.2981	0.1601	0.3124	0.4211	0.3127	0.1432	0.5132	3	broken bar

After inputting data into the neural network, comparative diagnosis is conducted to demonstrate the effectiveness of the improved method through data analysis. Using Matlab R2014a software, use the first 600 sets of feature vector data in Table 2 as the training data for the neural network, with 100 sets for each state. Use an improved particle swarm optimization algorithm to optimize the weight of the neural network. Select 601-700 sets of data in Table 2 as test data, with 20 sets for each state. The test results are shown in Fig. 6.

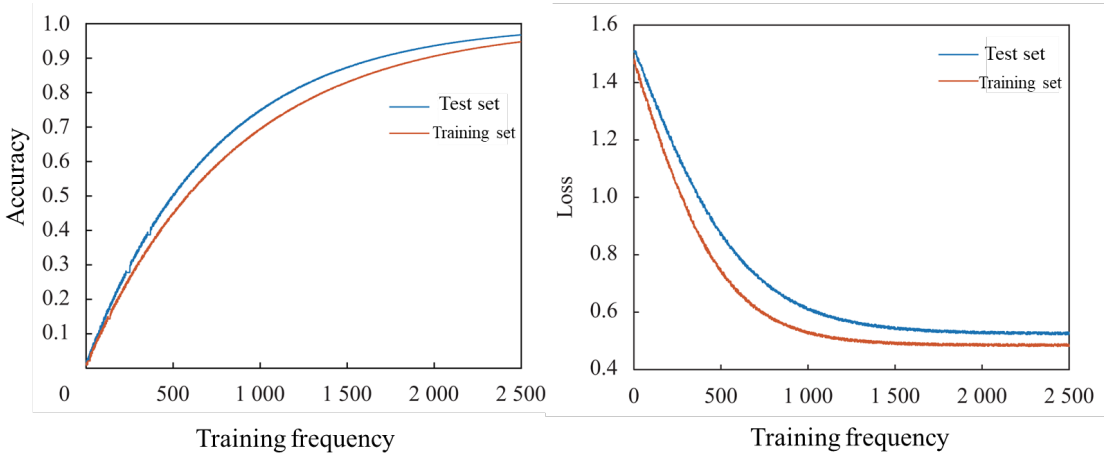

Fig. 6. Fault diagnosis schematic diagram

Through the above comparison, it can be seen that the improved algorithm has faster convergence speed and higher accuracy. The visualization results are shown in Fig. 7.

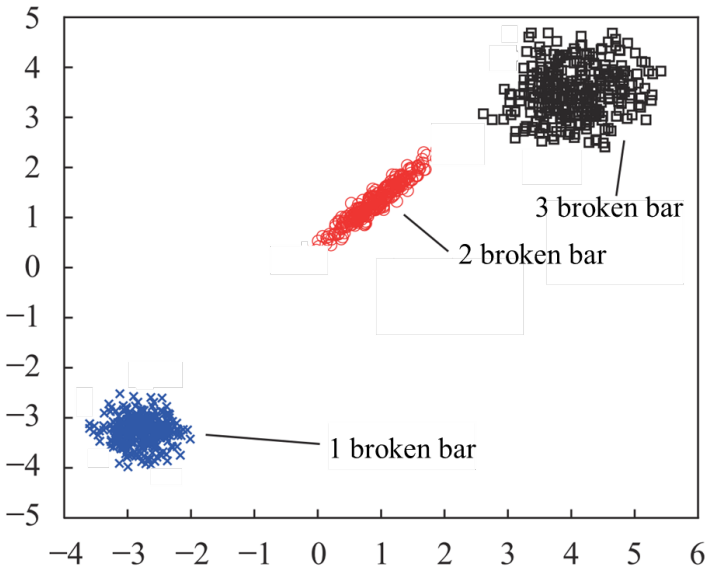

Fig. 7. Visualization results

Table 3. Recognition accuracy

Parameter	Accuracy	Test set	Validation set
	98.23%	95.32%	95.21%

After simulating the dataset, the convolutional neural network was trained to have the ability to diagnose faults in asynchronous motors. Then freeze the weights of the first few levels of the convolutional neural network model, train the weights of the fully connected layers using measured data, and fine tune the weight values using a smaller learning rate, ultimately minimizing the overall function. From Fig. 7 and Table 3, it can be seen that the improved method has achieved significant improvements in diagnostic speed and accuracy.

6 Conclusion

This article improves the diagnostic efficiency by studying three asynchronous motor faults. To this end, the main focus is on modeling motor faults. Then, the chaotic dynamic weighted particle swarm optimization algorithm is used to intelligently diagnose the motor model. Finally, the effectiveness of the algorithm is verified through experiments. The focus of future research will be on more comprehensive and diverse motor fault diagnosis to improve diagnostic accuracy.

7 Acknowledgement

Hebei Province Higher Education Science and Technology Research Project: Research on Surface Defect Detection System for Cold Rolled Strip Based on Deep Learning (ZC2021254).

References

[1] S. Marmouch, T. Aroui, Y. Koubaa, Statistical Neural Networks for Induction Machine Fault Diagnosis and Features Processing Based on Principal Component Analysis, IEEJ Transactions on Electrical and Electronic Engineering 16(2) (2021) 307-314.
[2] J. Kang, H. Im, Y. Oh, D. Kim, M. Park, J. Son, Motor fault diagnosis scheme by machine noise integration and signal similarity measurement, Journal of Advanced Marine Engineering and Technology (JAMET) 44(5)(2020) 405-413.
[3] J.-B. Wen, H.-Y. Zhao, Z.-N. Liu, Brushless DC motor sensor fault detection and fault-tolerant system based on neural network, Journal of Electronic Measurement and Instrumentation 32(10)(2018) 39-46.
[4] L. Han, J.-P. Guo, G.-H. Lu, Asynchronous Motor Fault Diagnosis Based on Improved BP Algorithm, Industrial Control Computer 34(2)(2021) 71-72.
[5] W.-W. Cai, J. Huang, W.-G. Li, X.-Z. Zhao, J.-R. Zhang, Z.-Z. Sun, Research on Fault Diagnosis Method for Micro Motor Based on Sound Signal, Machine Tool & Hydraulics 48(23)(2020) 190-195.
[6] X.-Z. Cheng, C.-A. Wang, J.-M. Li, C.-N. Xu, Motor fault diagnosis based on adaptive neural fuzzy Petri net algorithm, Journal of Shandong University of Science and Technology(Natural Science) 39(3)(2020) 109-117.
[7] D.-W. Meng, X.-H. Wang, Faultanalysis of Short Circuit Between Pieces of Large Motor Stator Cores, Journal of Harbin University of Science and Technology 25(3)(2020) 40-46.
[8] H. Zhang, Y.-L. Wang, T.-Z. Yong, H.-J. Ma, B.-X. Dai, Identification of Low Frequency Oscillation Signals Based on SVMD and Energy Transfer SR-MLS Inversion Recognition Technique, High Voltage Engineering 46(5)(2020) 1682-1692.
[9] J. Zhou, S. Wang, F.-Y. Liu, Research on Iris Recognition Algorithm Based on Wavelet Packet Decomposition, Computer Science 48(S1)(2021) 57-62.
[10] R. Song, Y.-X. Li, Infrared image enhancement based on improved quantum particle swarm optimization, Laser & Infrared 51(11)(2021) 1531-1537.